ARTICLES SCIENCE CHINA Materials

mater.scichina.com link.springer.com

Published online 7 November 2017 | doi: 10.1007/s40843-017-9139-8
Sci China Mater 2017, 60(12): 1168–1178

Fabrication of hybrid $Co_3O_4/NiCo_2O_4$ nanosheets sandwiched by nanoneedles for high-performance supercapacitors using a novel electrochemical ion exchange

Jiaxin Hao[1], Shanglong Peng[1*], Tianfeng Qin[1], Zilei Wang[1], Yuxiang Wen[1], Deyan He[1], Jiachi Zhang[1], Zhiya Zhang[1], Xiaoyan Fan[2] and Guozhong Cao[3*]

ABSTRACT **Electrochemical ion exchange has been used to tailor the composition of transition metal oxides (Co_3O_4) electrode with enhanced capacity while maintaining its crystal structure and morphology. Specifically, Ni ions were incorporated to Co_3O_4 nanosheets sandwiched by nanoneedles to form $Co_3O_4/NiCo_2O_4$ composite. As positive electrode for supercapacitors, the $Co_3O_4/NiCo_2O_4$ composite presents a high areal capacitance of 3.2 F cm^{-2} (1060 F g^{-1}) at a current density of 5 mA cm^{-2} and outstanding rate capability as well as long cycle stability. Moreover, the assembled aqueous asymmetric supercapacitor based on $Co_3O_4/NiCo_2O_4$//carbon cloth electrodes delivers a considerable energy density of 3.0 mW h cm^{-3} at power density of 136 mW cm^{-3}, and high rate capability (85% retention at a current density of 30 mA cm^{-2}). A safety light composed of ten green LEDs in parallel was lit for ~360 s using two identical supercapacitors in series, indicating a promising practical application.**

Keywords: electrochemical ion exchange, cobalt oxide, nickel cobalt oxide, asymmetric supercapacitors

INTRODUCTION

The development of efficient energy storage devices is gaining increasing attention due to their potential applications in the field of emergency power supplies and high power electronic devices [1–4]. Featured with high power density, long cycle stability and fast charge/discharge rates, supercapacitors (SCs) are regarded as one of the promising energy storage devices [2,5,6]. Despite these advantages, its relatively low energy density must be increased to satisfy their practical applications. Compared with conventional carbon materials featured with high conductivity and low electric double layer capacitance [1,7–9], the transition metal oxides/hydroxides (such as RuO_2, Co_3O_4, NiO, MnO_2 and $Ni(OH)_2$) present high pseudocapacitance through redox reactions taking place at the interface of electrode/electrolyte, which can enhance the energy density of device [10–14]. Among these electroactive materials, Co_3O_4 has dominated over other materials due to its low cost, simple synthetic process and extremely high theoretical capacitance (~3560 F g^{-1}) [15,16]. Unfortunately, the redox reaction is usually restricted by its intrinsic poor electrical conductivity and the sluggish ion diffusion near the electrode surface, leading to the lower observed capacitance values [17–20]. To tackle the problem, one of the promising methods is to introduce beneficial ions into Co_3O_4. Ni ion can be a representative of beneficial metal ions, and its introduction into the spinel Co_3O_4 can produce a nickel cobalt oxide composite, which exhibits the synergistic effect from Ni and Co ions, such as improved electrical conductivity and electrochemical performance [21–24]. More recently, different methods have been reported to synthesize nickel cobalt oxide with different nanostructure and morphology. For example, Jiao *et al.* [25] reported the partial substitution of Ni^{2+} in a Ni-MOF by active Co^{2+} *via* a hydrothermal method and the obtained CoNi-MOF exhibited a high specific capacity of 236.1 mA h g^{-1}

[1] Key Laboratory for Magnetism and Magnetic Materials of the Ministry of Education, School of Physical Science and Technology, Lanzhou University, Lanzhou 730000, China
[2] College of Mathematics and Physics, Qingdao University of Science and technology, Qingdao 266061, China
[3] Department of Materials Science and Engineering, University of Washington, Seattle, Washington 98195-2120, USA
[*] Corresponding authors (emails: pengshl@lzu.edu.cn (Peng S); gzcao@u.washington.edu (Cao G))

at a current density of 1 A g^{-1}; Zhang *et al.* [26] obtained core@shell Co_3O_4@$NiCo_2O_4$ nanowire arrays on Ni foam *via* a hydrothermal and co-electrodeposition method, exhibiting a high areal capacitance of 2.04 F cm^{-2} at a current density of 5 mA cm^{-2}. Wu *et al.* [22] reported mesoporous nickel cobalt oxide ($Ni_{0.3}Co_{2.7}O_4$) through calcining nickel cobalt oxalate hydrate, demonstrating a specific capacitance of 960 F g^{-1} at a current density of 0.625 A g^{-1}; These methods have demonstrated the successful preparation of nickel cobalt oxide; however, direct growth of hybrid $Co_3O_4/NiCo_2O_4$ on Ni foam for high performance supercapacitors has not been reported until now.

Herein, we reported a novel approach to synthesize $Co_3O_4/NiCo_2O_4$ nanosheets sandwiched by nanoneedles *via* combining hydrothermal and annealing treatment with a simple electrochemical ion exchange. Electrochemical ion exchange refers to the ion exchange that occurs under the action of electric field. Ion exchange can replace the Co^{2+} with Ni^{2+} and electric field can speed up the process. The fabrication of $Co_3O_4/NiCo_2O_4$ composite is derived from the partial substitution of Co^{2+} in the Co_3O_4 by active Ni^{2+} while the pristine crystal structure and morphology are remained [27,28]. Benefiting from the synergistic effect, the $Co_3O_4/NiCo_2O_4$ composite electrode delivers a high areal capacity of 3.2 F cm^{-2} at a current density of 5 mA cm^{-2} and excellent rate capability as well as long cycle stability. An asymmetric supercapacitor based on $Co_3O_4/NiCo_2O_4$//carbon cloth presents a high energy density of 3.0 mW h cm^{-3} at a power density of 136 mW cm^{-3} and good rate stability. Two devices in series light ten green LEDs in parallel for ~360 s, indicating a promising practical application.

EXPERIMENTAL SECTION

Synthesis of the Co_3O_4 nanosheets sandwiched by nanoneedles

All of the chemicals were analytical grade and used without further purification. The Co_3O_4 nanosheet sandwiched by nanoneedles was synthesized by a modified hydrothermal method in Teflon-line stainless-steel autoclave following an annealing process. Typically, 4.5 mmol of $Co(NO_3)_2{\cdot}6H_2O$, 4 mmol of NH_4F and 20 mmol of urea were dissolved in 45 mL of distilled water and stirred for 20 min to obtain a homogeneous aqueous solution. Next, Ni foam (2 cm×5 cm×0.1 cm) was degreased and cleaned with acetone, HCl (6 mol L^{-1}), alcohol and DI in an ultrasound bath for 20 min, respectively. After that, the prepared solution and the refreshed Ni foam were moved into an autoclave with the capacity of 60 mL, maintained at 110°C for 6 h. Following, the Ni foam coated with pink precursors was rinsed with distilled water and ethanol, and then dried at 60°C for 6 h. Finally, the obtained sample was put into a tube furnace at 300°C for 2 h in air to obtain the sample of Co_3O_4. The mass loading of Co_3O_4 on Ni foam is about 3 mg cm^{-2}.

Synthesis of the hybrid $Co_3O_4/NiCo_2O_4$ nanosheets sandwiched by nanoneedles

$NiCl_2{\cdot}6H_2O$ (0.84 mol L^{-1}) was dissolved in 40 mL of distilled water and stirred to form a homogeneous solution. A Ti plate (1 cm×1 cm) and the Ni foam coated with Co_3O_4 were used as the counter and working electrodes, respectively. At the same time the electrolyte was maintained at 55°C. Then, a current density of 10 mA cm^{-2} was used in two electrode systems for 60 s. Next, the obtained samples were washed with alcohol for three times and then dried at 60°C for 6 h. Compared with the pure Ni foam, the total mass loading after electrochemical treatment is about 3.05 mg cm^{-2}.

Assembly of $Co_3O_4/NiCo_2O_4$//carbon cloth asymmetric supercapacitors

The asymmetric supercapacitor (ASC) was fabricated by assembling with $Co_3O_4/NiCo_2O_4$ electrode as the positive electrode, carbon cloth (Shanghai Lishuo Composite Material Technology Co., Ltd., Shanghai 200335, China.) as the negative electrode, cellulose paper as the separator and the KOH (1 mol L^{-1}) aqueous solution as electrolyte.

In order to meet the charge balance, the area ratio of the $Co_3O_4/NiCo_2O_4$ electrode and carbon cloth electrode should follow the equation [18]:

$$A_+ / A_- = (C_- \times \Delta V_-) / (C_+ \times \Delta V_+), \quad (1)$$

where A is the active area of the electrode, ΔV is the potential range for the discharging process and C is the areal capacitance of the electrode material. Considering the equation above, the area ratio of $Co_3O_4/NiCo_2O_4$ to carbon cloth is calculated to be 1:0.6.

Material characterizations

The microstructure and morphology were investigated by field emission scanning electron microscopy (FE-SEM, Hitachi S-4800) and transmission electron microscopy (TEM, FEI Tecnai F30, operated at 300 kV). The chemical component was analyzed on a multifunctional X-ray photoelectron spectroscope (XPS, PHI-5702, Mg Kα X-ray, 1253.6 eV). The crystal structure of the samples was

determined using X-ray diffraction (XRD, Cu Kα irradiation, λ=0.154056 nm) with a SIEMENS D5000 X-ray diffractometer.

Electrochemical measurements

The electrochemical tests were carried out in a three-electrode system in 1 mol L^{-1} KOH electrolyte. The sample, Pt plate and Ag/AgCl were used as working electrode, counter electrode and reference electrode, respectively. The electrochemical performances were tested in an electrochemical workstation (CHI660E, CH Instrument In., Shanghai) by the techniques of electrochemical impedance spectroscopy (EIS), cyclic voltammetry (CV) and galvanostatic charge-discharge (GCD).

The areal capacitances C were calculated from GCD curves according to the equation [3]:

$$C = I \times \Delta t / (S \times \Delta V), \quad (2)$$

where I is the constant discharge current density, Δt the discharge time, S the area of the active electrode and ΔV the voltage drop upon discharging.

The specific capacitances C_m were calculated from areal capacitance C according to the equation:

$$C_m = C / m, \quad (3)$$

where m is weight of the active electrode material.

The energy density (E) and power density (P) of the device are calculated according to the equations below [29]:

$$E = C \times \Delta V^2 / (2 \times 3.6), \quad (4)$$

$$P = E \times 3600 / \Delta t, \quad (5)$$

where C is the areal capacitance of the ASC, V the effective volume of the ASC, ΔV the operating voltage window and Δt the discharge time.

RESULTS AND DISSCUSSION

Morphology and structure

Fig. 1 illustrates the formation process of the hybrid $Co_3O_4/NiCo_2O_4$ nanocomposites. The Co_3O_4 nanosheets sandwiched by nanoneedles were firstly grown on the Ni foam substrate by a facile hydrothermal treatment and followed with annealing treatment. The formation mechanism of the unique nanostructure can be explained as follows [30]. The ammonium fluoride is hydrolyzed to generate hydrofluoric acid and ammonia in hot water forming a strongly acidic system. Compared with nanosheets, the nanoneedles are much easier to be etched by strong acid, which caused the formation of nanosheets in the early stages of the reaction. When the reaction is proceeding, the ammonium fluoride is gradually consumed, resulting in the formation of nanoneedles. Eventually, the unique 3D nanosheets sandwiched by nanoneedles are formed. Then, the as-prepared Co_3O_4 sample was treated using the electrochemical ion exchange in $NiCl_2$ solution to obtain hybrid $Co_3O_4/NiCo_2O_4$ nanosheets while maintaining its pristine morphology.

For the Co_3O_4 sample, the low-magnification SEM image (Fig. 2a) shows a typical 3D structure with the vertical nanosheets growing densely and homogeneously on the surface of Ni foam over a large-scale. As presented in the Fig. 2b for the high magnification, it can be observed that each of Co_3O_4 nanosheet is sandwiched by interconnected and overlapped nanoneedles, which can effectively increase the specific surface of the electrode. Moreover, such 3D nanostructure can contribute to the easy accessibility of electrolyte ions to the surface of active materials, resulting in the enhancement of the electrochemical properties [27,29]. The TEM image in Fig. 2c demonstrates that the Co_3O_4 nanoneedle with the diameter of ~70 nm is composed of interconnected nanocrystallites with the diameters ranging from 8 to 12 nm. The gap between the nanocrystallites can serve as ion transfer speedways and shorten the diffusion distance of electrolyte ions, which is beneficial for the enhancement of rate capability [21]. The lattice fringes with the interplanar spacing of 0.285 nm could be clearly observed in high-resolution TEM (HRTEM) image as shown in the inset of Fig. 2c, corresponding to the (220) lattice plane of Co_3O_4 crystals. As shown in Fig. 2d, XRD measurement

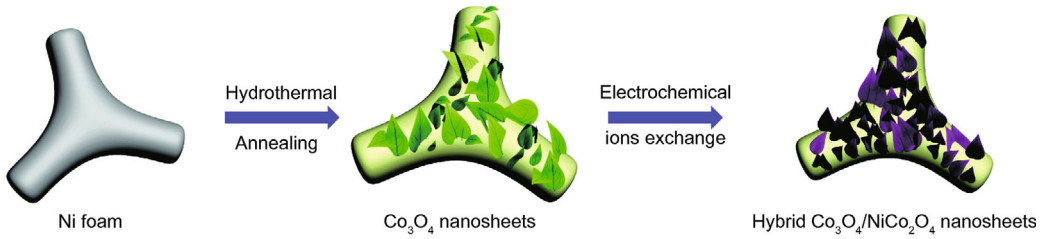

Figure 1 Schematic illustration of the fabrication process for $Co_3O_4/NiCo_2O_4$ nanosheets sandwiched by nanoneedles grown on Ni foam.

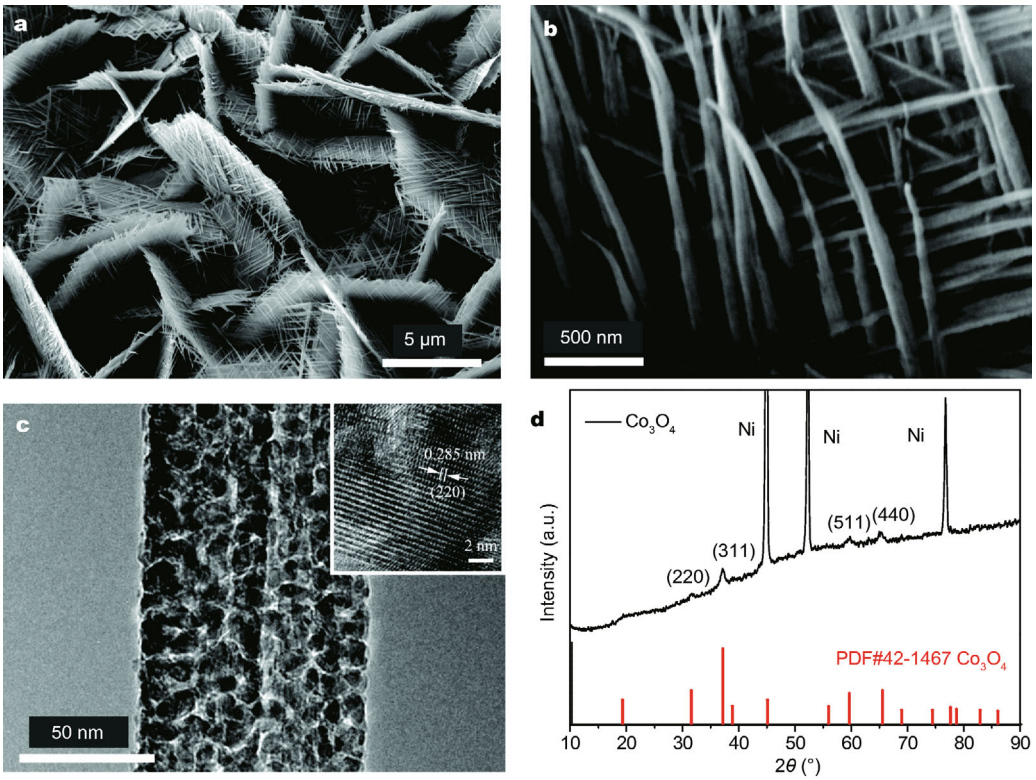

Figure 2 SEM (a, b) and TEM images (c) of Co_3O_4 sample (inset: HRTEM image), XRD pattern of the Co_3O_4 sample (d).

was employed to further confirm the synthesis of Co_3O_4. Three strong diffraction peaks are located at 44.4°, 51.6° and 76.1°, respectively, which are ascribed to the Ni foam substrate. The other diffraction peaks are observed at 31.2°, 36.8°, 59.3° and 65.2°, which could be identified as (220), (311), (511) and (400) crystal planes of Co_3O_4 (JCPDS No. 42-1467), respectively, in accordance with the result of HRTEM.

After electrochemical treatment, the morphology and structure of the sample was characterized by SEM and shown in Fig. 3a, b. Compared Fig 2a, b for Co_3O_4 with Fig 3a, b for $Co_3O_4/NiCo_2O_4$, little changes can be observed, indicating that the electrochemical ions exchange hardly affect its initial morphology. To confirm the formation of $Co_3O_4/NiCo_2O_4$, a series of characterizations were carried out. As shown in Fig. 3c, the TEM image of $Co_3O_4/NiCo_2O_4$ reveals that there is no other substance on the surface after electrochemical ion exchange. Besides, the surface becomes unclear due to the desorption of Co^{2+} and the adsorption of Ni^{2+}. The HRTEM (inset) reveals that the lattice fringe spacing is 0.245 nm, close to the theoretical interplanar spacing of spinel $NiCo_2O_4$ (311) planes, indicating the existence of $NiCo_2O_4$. The composition of the as-prepared sample was confirmed by energy-dispersive X-ray spectrometer (EDX) (Fig. S1) and the atom ratio of Ni:Co is about 0.8:2.2, which is lower than the stoichiometric ratio of Ni/Co in $NiCo_2O_4$. According to the previously reported literature, Co ions of the spinel Co_3O_4 can be replaced by Ni ions to form $NiCo_2O_4$ [15]. However, when the reaction is insufficient, there is the partial existence of Co_3O_4, leading to the deviation of the stoichiometric ratio of Co/Ni and the formation of hybrid $Co_3O_4/NiCo_2O_4$. Moreover, the crystal phase change of nickel cobalt oxide was investigated by XRD analysis as presented in Fig. 3d. All of these identified peaks are indexed to the standard patterns of $NiCo_2O_4$ (JCPDS No. 42-1457) and Co_3O_4 (JCPDS No. 42-1467), indicating that the introduction of nickel ions does not change the spinel structure of the samples [21,31]. According to the results above, it can be concluded that partial Co ions of the spinel Co_3O_4 are replaced by Ni ions during the electrochemical process while maintaining its crystal structure and morphology, which lead to the formation of the hybrid spinel $Co_3O_4/NiCo_2O_4$ nanocomposites [22,23,27,28].

XPS test was used to further confirm the surface elemental composition of the $Co_3O_4/NiCo_2O_4$ and the results are presented in Fig. 4. The peak signals of Co 2p,

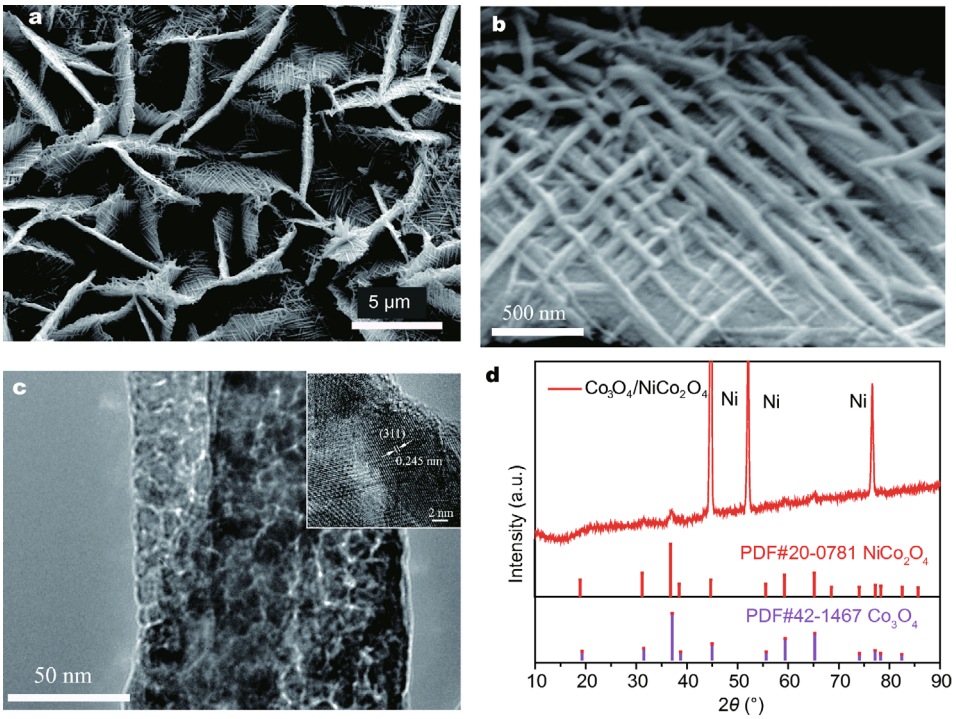

Figure 3 SEM (a, b) and TEM images (c) of $Co_3O_4/NiCo_2O_4$ sample (inset: HRTEM image), XRD pattern of the $Co_3O_4/NiCo_2O_4$ composite (d).

Ni 2p and O 1s can be obviously observed in Fig. 4a. As displayed in Fig. 4b, the characteristic peaks of Co 2p spectrum accompanied by two shakeup satellite peaks (Sat) are clearly discerned, and it is successfully divided into four peaks at 781.2/793.3 eV and 779.9/794.9 eV by using Lorentzian-Gaussian fitting method, which are the existing proof of Co^{2+} and Co^{3+}, respectively [15,32]. As for the spectrum of Ni 2p (Fig. 4c), there are also two main spin-orbital peaks (Ni $2p_{3/2}$ and Ni $2p_{1/3}$ at 854.8 and 872.4 eV, respectively) and two shakeup satellites and the results are consistent with other reports, indicating the presences of Ni^{2+} and Ni^{3+} [33,34]. The existent of Ni^{3+} may stem from the defect and cation vacancy of Co^{3+} [21]. These results confirm the transformation from Co_3O_4 to the $NiCo_2O_4$, corresponding to the results of high-magnification TEM and XRD. In Fig. 4d, the spectrum of O 1s was divided into four components. The O1 peak located at 529.4 eV is attributed to metal-oxygen bonds, suggesting the presence of Ni–Co–O; the O2 peak centered at 531.2 eV is usually ascribed to the presence of defect sites with minimum oxygen coordination of the material; the O3 and O4 peaks can be associated with the oxygen in hydroxyl group on the surface of sample and the physically adsorbed or chemisorbed water, respectively [35,36].

Electrochemical performance

To highlight the merits of our electrode design, both of the Co_3O_4 and $Co_3O_4/NiCo_2O_4$ were tested as the positive electrode in a three-electrode system in 1 mol L^{-1} KOH electrolyte. Fig. 5a presents the CV curves of the pristine Co_3O_4 and $Co_3O_4/NiCo_2O_4$ electrodes at a scan rate of 10 mV s^{-1}. The redox peaks are obvious in the CV plots of both electrodes, indicating the pseudocapacitance of Co_3O_4 and $Co_3O_4/NiCo_2O_4$. Compared with the pure Co_3O_4 electrode, the hybrid $Co_3O_4/NiCo_2O_4$ electrode shows stronger redox peaks, which are associated with the Faradaic redox reactions related to M–O/M–O–OH, where M refers to Ni or Co while the redox peaks of Co_3O_4 only come from Co [14]. Fig. 5b represents the GCD curves of the Co_3O_4 and $Co_3O_4/NiCo_2O_4$ electrodes at a current density of 1 mA cm^{-2}. It can be observed that the $Co_3O_4/NiCo_2O_4$ exhibits slower and more linear variation of potential *vs.* time, confirming the enhanced pseudocapacitance. Fig. 5c shows the CV curves of the $Co_3O_4/NiCo_2O_4$ electrode at various scan rates ranging from 10 to 50 mV s^{-1}. A pair of redox peaks can be even observed at a high scan rates, which reveals that the $Co_3O_4/NiCo_2O_4$ electrode is favorable for fast redox reaction and ions diffusion [37,38]. With the increase of scan rates, the anodic peak shifted to higher potential

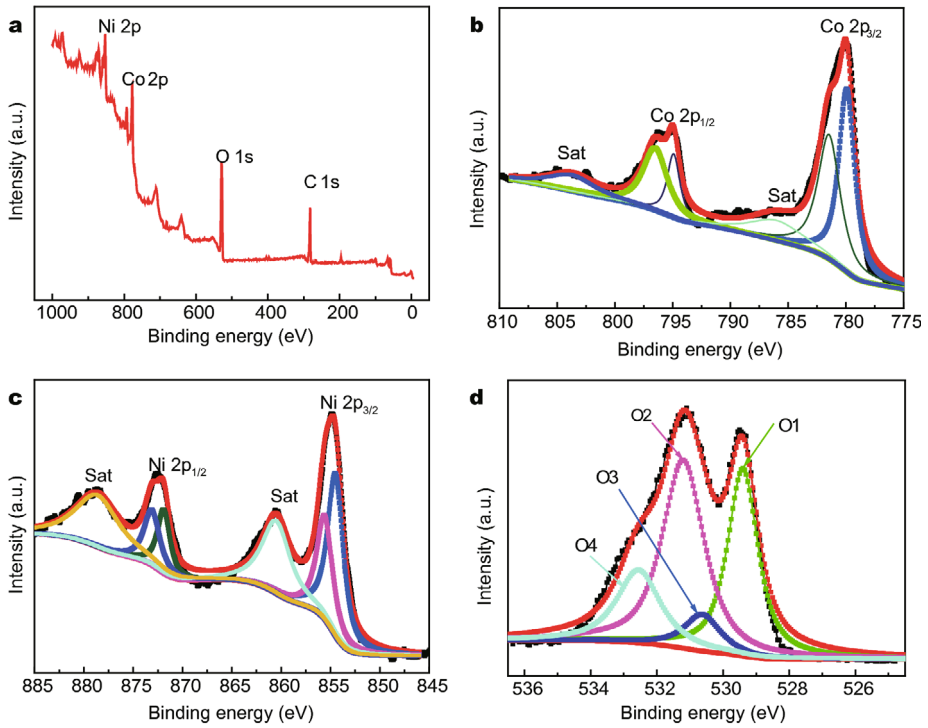

Figure 4 XPS spectra of $Co_3O_4/NiCo_2O_4$ nanosheets. The entire spectrum (a) and the narrow spectra of Co 2p (b), Ni 2p (c) and O 1s (d).

while the cathodic peak shifted to lower potential. This is mainly derived from the internal resistance of the electrode and the polarization caused by high scan rates [21,39]. Fig. 5d provides the GCD profiles of the $Co_3O_4/NiCo_2O_4$ electrode at different current densities ranging from 1 to 50 mA cm^{-2}. The charging and discharging curves show fairly linear slopes at 0.4 and 0.35 V, respectively, confirming again the superior pseudocapacitance, which is consistent with CV curves. Moreover, even at high current density, the GCD curves are still highly symmetric, indicating an excellent electrochemical reversibility of $Co_3O_4/NiCo_2O_4$ electrode. According to the GCD curves, the areal capacitances of the $Co_3O_4/NiCo_2O_4$ electrode at different current densities were calculated and shown in Fig. 5e. The areal capacitances of 3.2 (~1060 F g^{-1}), 3.1 and 2.8 F cm^{-2} are obtained at the current densities of 5, 10 and 30 mA cm^{-2}, respectively. Typically, the highest areal capacitance of the $Co_3O_4/NiCo_2O_4$ electrode is 3.3 F cm^{-2} (~1080 F g^{-1}) with a high mass loading of ~3.05 mg cm^{-2} at a current density of 1 mA cm^{-2}, almost four times of the pristine Co_3O_4 electrode (0.80 F cm^{-2}). In comparison with the pristine Co_3O_4 electrode, the hybrid $Co_3O_4/NiCo_2O_4$ electrode shows an immense enhancement of the areal capacitances, which is due to: (1) the synergistic effect of Co_3O_4 and $NiCo_2O_4$ provides richer redox chemistry than individual binary oxide, leading to a higher specific capacity; (2) the activity of Co ion could be significantly increased by Ni ions in ternary oxide, resulting in the enhancement of electrochemical performance [40]; (3) the enhanced conductivity caused by the introduction of Ni ions [41]. Besides, the capacity is much higher than those of the previously reported nickel cobalt oxide electrodes such as 2.01 F cm^{-2} for $NiCo_2O_4$ nanowires [42], 2.04 F cm^{-2} for Co_3O_4@$NiCo_2O_4$ nanowires [26], which can be attributed to the reasonable design of hybrid $Co_3O_4/NiCo_2O_4$. A capacitance retention of 84% is obtained for the $Co_3O_4/NiCo_2O_4$ electrode at a high current density of 30 mA/cm^2, indicative of excellent rate capability. Compared with the pristine Co_3O_4 electrode (69% retention at current density of 50 mA cm^{-2}), the 74% retention for the $Co_3O_4/NiCo_2O_4$ electrode at the same current density indicates the importance of Ni ion in enhancing the rate stability. In addition, the rate stability is also much better than those of the reported Co-Co_3O_4 nanowires (57.1% at current density of 40 mA cm^{-2}) [43] and $NiCo_2O_4$@rGO hybrid nanostructures (82% at current density of 20 mA cm^{-2}) [44], which may be ascribed to the unique 3D structure of the combination of nanosheets and nanoneedles. The Nyquist plots of $Co_3O_4/$

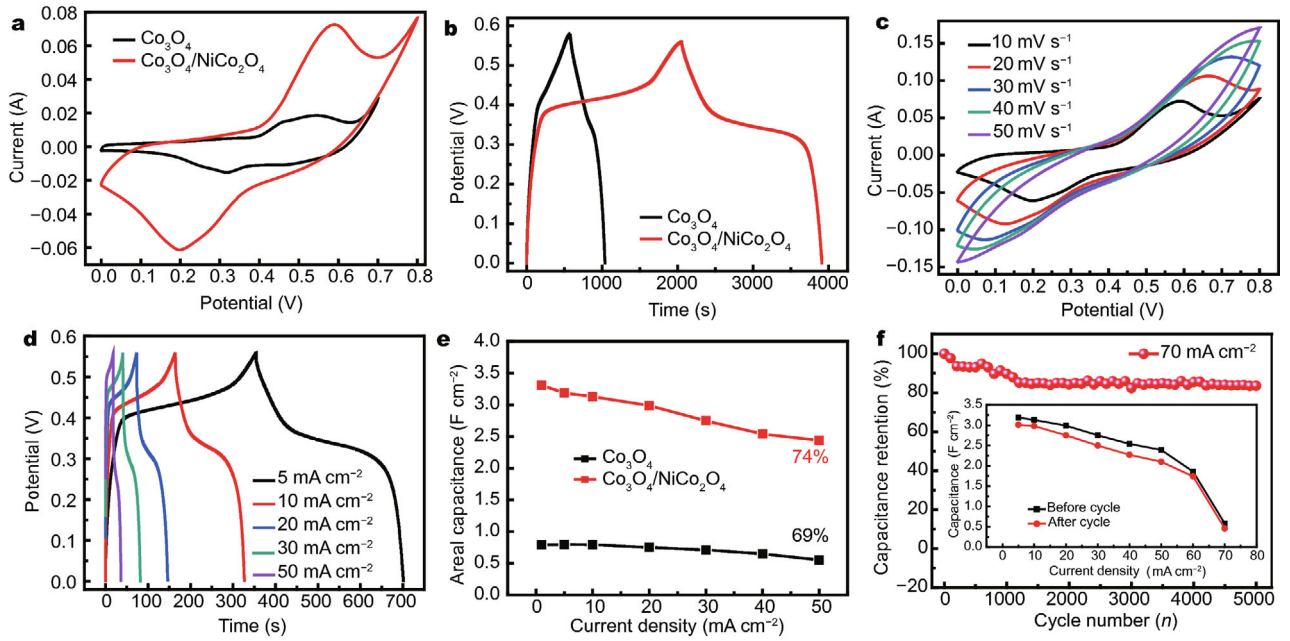

Figure 5 Electrochemical performance of Co_3O_4 and hybrid $Co_3O_4/NiCo_2O_4$. CV curves at a scan rate of 10 mV s^{-1} (a) and GCD curves at a current density of 1 mA cm^{-2} (b) of the pristine Co_3O_4 and $Co_3O_4/NiCo_2O_4$ electrodes; CV curves (c) and GCD curves (d) of $Co_3O_4/NiCo_2O_4$ electrode; areal capacitance as a function of current density for the pristine Co_3O_4 and $Co_3O_4/NiCo_2O_4$ electrodes (e); cycling stability of the $Co_3O_4/NiCo_2O_4$ electrode at a current density of 70 mA cm^{-2}, inset: the areal capacitances of $Co_3O_4/NiCo_2O_4$ electrode at different current densities before and after testing (f).

$NiCo_2O_4$ and Co_3O_4 electrodes and the equivalent circuit diagram used for fitting the EIS data are displayed in Fig. S2. The equivalent circuit includes internal resistance R_s, charge transfer resistance R_{ct} and the electric double layer capacitance C_{dl}. The fitted values are shown in Table S1. In the low frequency region, they have a similar vertical line, indicating a more ideal capacitive property [45]. In the high frequency region, the internal resistance of the $Co_3O_4/NiCo_2O_4$ (0.25 Ω) is lower than that of the pristine Co_3O_4 electrode (2.31 Ω), which is deduced by the introduction of the Ni ions. Moreover, the R_{ct} of the $Co_3O_4/NiCo_2O_4$ is 1.96 Ω, smaller than that of the Co_3O_4 (2.85 Ω), confirming that the hybrid nanostructure of the Co_3O_4 and $NiCo_2O_4$ electrode can effectively reduce the charge transfer resistance. As shown in Fig. 5f, the cycling stability of the $Co_3O_4/NiCo_2O_4$ electrode was examined using GCD test at a high current density of 70 mA cm^{-2} for 5000 cycles. The capacitance retention is 84% after 5000 cycles, indicating a good cycling stability. The insert section shows the areal capacitances of $Co_3O_4/NiCo_2O_4$ electrode at different current densities before and after cycle test and the slight change confirms again the excellent cycling stability of the electrode.

To further investigate the energy storage capacity of the $Co_3O_4/NiCo_2O_4$ electrode for practical applications, an asymmetric supercapacitor (ASC) was assembled using the $Co_3O_4/NiCo_2O_4$ electrode as the positive electrode (1 cm×1 cm×0.1 cm), commercial carbon cloth (1 cm×0.6 cm×0.05 cm) as the negative electrode and 1 mol L^{-1} KOH aqueous solution as the electrolyte (Fig. 6a). The commercial carbon cloth was directly used as the negative electrode material without any treatment. In our previous work, the electrochemical properties of this carbon cloth have been studied in detail [46] and its CV and GCD curves are shown in Fig. S3. Fig. S4 shows the CV curves of the carbon cloth and $Co_3O_4/NiCo_2O_4$ electrode at a scan rate of 10 mV s^{-1}, which confirm that the ASC can operate at the voltage of 1.6 V. Fig. 6b presents the CV curves of the device at different scan rates with the voltage window ranging from 0 to 1.6 V. The irregular shape is caused by the double contribution of electric double-layer capacitance and pseudocapacitance, which derive from the carbon cloth and active materials, respectively [47]. With the increasing scan rates from 10 to 100 mV s^{-1}, no obvious distortion can be observed in the CV curves, confirming the rapid ions diffusion in the aqueous electrolyte. GCD curves of ASC at a series of current densities ranging from 1 to 30 mA cm^{-2} are illustrated in Fig. 6c. The areal capacitances of the ASC reached 1.2, 1.1 and 0.7 F cm^{-2} at current densities of 1, 10 and 50 mA cm^{-2},

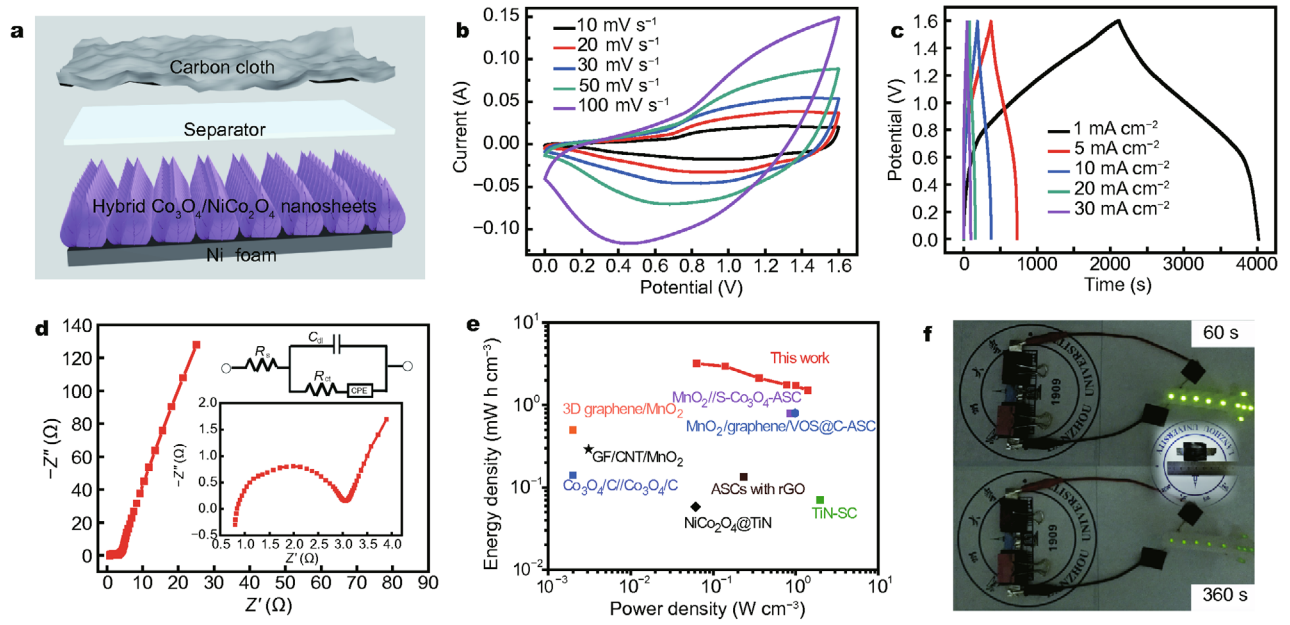

Figure 6 Electrochemical performances of ASC based on $Co_3O_4/NiCo_2O_4$//carbon cloth. Schematic illustration of the device structure for the device (a); CV curves of the ASC at various scan rates (b); GCD curves of the ASC at different current densities (c); Nyquist plot for the device recorded from 0.01 Hz to 1 MHz and equivalent circuit diagram used for fitting the EIS (d); comparison in a Ragone plot of the volumetric energy densities and power densities reported in previous references and those of our ASC device (e); image of a safety light composed of ten green LEDs in parallel lighted by two ASCs in series (f).

respectively. It is noteworthy that the areal capacitance of ASC retains 58.3% of its initial capacitance at the current density of 50 mA cm^{-2} as shown in Fig. S5, and the capacitance still remains at 45.0% even at large current density of 150 mA cm^{-2}, demonstrating extremely superior rate stability. To further investigate the electrochemical properties of the asymmetric device, the Nyquist plot is fitted according to the equivalent circuit in Fig. 6d. CPE is the constant phase elements and is used to offset the nonhomogeneity of the system. In the low-frequency portion, the slope of the curve is more than 79°, revealing the fast electrolyte diffusion in the asymmetric device [3]. The EIS fitting results reveal that the internal resistance and the charge-transfer resistance are 1.14 Ω and 4.38 Ω, respectively, reflecting good interfacial contact between the electro-active material and the current collector and rapid ions transfer in the electrode material [48]. The result is consistent with the outstanding rate stability of the device. To further investigate its practical application, the volumetric power and energy density of the ASC were calculated from GCD curves. The maximum energy density is 3.0 mW h cm^{-3} at a power density of 136 mW cm^{-3}. Even at a high discharge current of 150 mA cm^{-2}, the energy density can still remain 1.5 mW h cm^{-3} at a power density of 1.4 W cm^{-3}, which is higher than those of the recently reported devices and the details are shown in Fig. 6e [10,15,18,49–53]. Fig. S5c shows the cycle test of ASC under continuous charge-discharge tests at a current density of 70 mA cm^{-2}. The capacity retention of the device is 81.4% after 5000 cycles, demonstrating excellent cycling stability. To demonstrate the practicability and operability of our ASC, a safety light composed of ten LEDs in parallel was powered by two $Co_3O_4/NiCo_2O_4$//carbon cloth devices in series for 360 s after charging to 3.2 V within 3 min (Fig. 6f).

CONCLUSIONS

We have designed and fabricated a $Co_3O_4/NiCo_2O_4$ composite electrode through combining the hydrothermal and annealing treatments with a novel electrochemical ion exchange. The $Co_3O_4/NiCo_2O_4$ composite was obtained by the partial substitution of Co^{2+} of the Co_3O_4 with active Ni^{2+}. When used as positive electrode, the composite electrode exhibits high capacity, good rate capability and cycling stability. The good electrochemical performances are attributed to the synergistic effect between Co_3O_4 and $NiCo_2O_4$, which could provide richer redox chemistry than individual binary oxide, leading to higher specific capacity. Moreover, the well-designed composite electrode could provide good electron and ion

transport pathways, resulting in rapid and effective redox reactions. When evaluated as an electrode material for asymmetric supercapacitor, the as-fabricated Co_3O_4/$NiCo_2O_4$//carbon cloth device presented a high energy density of 3.0 mW h cm^{-3} at a power density of 136 mW cm^{-3} and high rate stability. Two devices in series light ten green LEDs in parallel for ~360 s, indicating a promising practical application. This work also opens new opportunities for rational design of composite metal oxide for high-performance electrochemical storage system.

Received 4 August 2017; accepted 28 September 2017; published online 7 November 2017

1 Wang G, Zhang L, Zhang J. A review of electrode materials for electrochemical supercapacitors. Chem Soc Rev, 2012, 41: 797–828
2 Guo K, Ma Y, Li H, *et al.* Flexible wire-shaped supercapacitors in parallel double helix configuration with stable electrochemical properties under static/dynamic bending. Small, 2016, 12: 1024–1033
3 Zhang S, Pan N. Supercapacitors performance evaluation. Adv Energ Mater, 2015, 5: 1401401
4 Lee KK, Chin WS, Sow CH. Cobalt-based compounds and composites as electrode materials for high-performance electrochemical capacitors. J Mater Chem A, 2014, 2: 17212–17248
5 Salanne M, Rotenberg B, Naoi K, *et al.* Efficient storage mechanisms for building better supercapacitors. Nat Energy, 2016, 1: 16070
6 Zhang X, Zhang H, Lin Z, *et al.* Recent advances and challenges of stretchable supercapacitors based on carbon materials. Sci China Mater, 2016, 59: 475–494
7 Cheng H, Hu C, Zhao Y, *et al.* Graphene fiber: a new material platform for unique applications. NPG Asia Mater, 2014, 6: e113
8 Qin T, Liu B, Wen Y, *et al.* Freestanding flexible graphene foams@polypyrrole@MnO_2 electrodes for high-performance supercapacitors. J Mater Chem A, 2016, 4: 9196–9203
9 Candelaria SL, Uchaker E, Cao G. Comparison of surface and bulk nitrogen modification in highly porous carbon for enhanced supercapacitors. Sci China Mater, 2015, 58: 521–533
10 Lu X, Wang G, Zhai T, *et al.* Stabilized TiN nanowire arrays for high-performance and flexible supercapacitors. Nano Lett, 2012, 12: 5376–5381
11 Zhi M, Xiang C, Li J, *et al.* Nanostructured carbon-metal oxide composite electrodes for supercapacitors: a review. Nanoscale, 2013, 5: 72–88
12 Wen Y, Qin T, Wang Z, *et al.* Self-supported binder-free carbon fibers/MnO_2 electrodes derived from disposable bamboo chopsticks for high-performance supercapacitors. J Alloys Compd, 2017, 699: 126–135
13 Tan Q, Wang P, Liu H, *et al.* Hollow MO_x-RuO_2 (M=Co, Cu, Fe, Ni, CuNi) nanostructures as highly efficient electrodes for supercapacitors. Sci China Mater, 2016, 59: 323–336
14 Nie Z, Wang Y, Zhang Y, *et al.* Multi-shelled α-Fe_2O_3 microspheres for high-rate supercapacitors. Sci China Mater, 2016, 59: 247–253
15 Zhang C, Xiao J, Lv X, *et al.* Hierarchically porous Co_3O_4/C nanowire arrays derived from a metal-organic framework for high performance supercapacitors and the oxygen evolution reaction. J Mater Chem A, 2016, 4: 16516–16523
16 Xia X, Tu J, Zhang Y, *et al.* Freestanding Co_3O_4 nanowire array for high performance supercapacitors. RSC Adv, 2012, 2: 1835–1841
17 Zhang F, Yuan C, Lu X, *et al.* Facile growth of mesoporous Co_3O_4 nanowire arrays on Ni foam for high performance electrochemical capacitors. J Power Sources, 2012, 203: 250–256
18 Xu W, Chen J, Yu M, *et al.* Sulphur-doped Co_3O_4 nanowires as an advanced negative electrode for high-energy asymmetric supercapacitors. J Mater Chem A, 2016, 4: 10779–10785
19 Wen Y, Peng S, Wang Z, *et al.* Facile synthesis of ultrathin $NiCo_2S_4$ nano-petals inspired by blooming buds for high-performance supercapacitors. J Mater Chem A, 2017, 5: 7144–7152
20 Yuan C, Yang L, Hou L, *et al.* Growth of ultrathin mesoporous Co_3O_4 nanosheet arrays on Ni foam for high-performance electrochemical capacitors. Energ Environ Sci, 2012, 5: 7883
21 Jiang Y, Zhang L, Zhang H, *et al.* Hierarchical $Ni_{0.54}Co_{0.46}O_2$ nanowire and nanosheet arrays grown on carbon fiber cloth for high-performance supercapacitors. J Power Sources, 2016, 329: 473–483
22 Wu HB, Pang H, Lou XWD. Facile synthesis of mesoporous $Ni_{0.3}Co_{2.7}O_4$ hierarchical structures for high-performance supercapacitors. Energ Environ Sci, 2013, 6: 3619
23 Wang H, Gao Q, Jiang L. Facile approach to prepare nickel cobaltite nanowire materials for supercapacitors. Small, 2011, 7: 2454
24 Yuan C, Li J, Hou L, *et al.* Ultrathin mesoporous $NiCo_2O_4$ nanosheets supported on Ni foam as advanced electrodes for supercapacitors. Adv Funct Mater, 2012, 22: 4592–4597
25 Jiao Y, Pei J, Chen D, *et al.* Mixed-metallic MOF based electrode materials for high performance hybrid supercapacitors. J Mater Chem A, 2017, 5: 1094–1102
26 Zhang G, Wang T, Yu X, *et al.* Nanoforest of hierarchical Co_3O_4@$NiCo_2O_4$ nanowire arrays for high-performance supercapacitors. Nano Energy, 2013, 2: 586–594
27 Zhou W, Liu X, Sang Y, *et al.* Enhanced performance of layered titanate nanowire-based supercapacitor electrodes by nickel ion exchange. ACS Appl Mater Interfaces, 2014, 6: 4578–4586
28 Wei W, Mi L, Gao Y, *et al.* Partial ion-exchange of nickel-sulfide-derived electrodes for high performance supercapacitors. Chem Mater, 2014, 26: 3418–3426
29 Kong D, Cheng C, Wang Y, *et al.* Three-dimensional Co_3O_4@C@Ni_3S_2 sandwich-structured nanoneedle arrays: towards high-performance flexible all-solid-state asymmetric supercapacitors. J Mater Chem A, 2015, 3: 16150–16161
30 Lin L, Liu J, Liu T, *et al.* Growth-controlled $NiCo_2S_4$ nanosheet arrays with self-decorated nanoneedles for high-performance pseudocapacitors. J Mater Chem A, 2015, 3: 17652–17658
31 Zhang Q, Zhao B, Wang J, *et al.* High-performance hybrid supercapacitors based on self-supported 3D ultrathin porous quaternary Zn-Ni-Al-Co oxide nanosheets. Nano Energy, 2016, 28: 475–485
32 Yang Y, Zhou M, Guo W, *et al.* $NiCoO_2$ nanowires grown on carbon fiber paper for highly efficient water oxidation. Electrochim Acta, 2015, 174: 246–253
33 Chen S, Yang G, Jia Y, *et al.* Three-dimensional $NiCo_2O_4$@$NiWO_4$ core-shell nanowire arrays for high performance supercapacitors. J Mater Chem A, 2017, 5: 1028–1034
34 Zhang L, Zhang D, Ren Z, *et al.* Mesoporous $NiCo_2O_4$ micro/nanospheres with hierarchical structures for supercapacitor and methanol electro-oxidation. ChemElectroChem, 2017, 4: 441–449,
35 Sun S, Wang S, Li S, *et al.* Asymmetric supercapacitors based on a $NiCo_2O_4$/three dimensional graphene composite and three di-

mensional graphene with high energy density. J Mater Chem A, 2016, 4: 18646–18653
36 Chen R, Wang HY, Miao J, *et al.* A flexible high-performance oxygen evolution electrode with three-dimensional $NiCo_2O_4$ core-shell nanowires. Nano Energy, 2015, 11: 333–340
37 Lu XF, Wu DJ, Li RZ, *et al.* Hierarchical $NiCo_2O_4$ nanosheets@hollow microrod arrays for high-performance asymmetric supercapacitors. J Mater Chem A, 2014, 2: 4706–4713
38 Wang K, Zhang X, Sun X, *et al.* Conducting polymer hydrogel materials for high-performance flexible solid-state supercapacitors. Sci China Mater, 2016, 59: 412–420
39 Zhou M, Lu F, Shen X, *et al.* One-pot construction of three dimensional $CoMoO_4/Co_3O_4$ hybrid nanostructures and their application in supercapacitors. J Mater Chem A, 2015, 3: 21201–21210
40 Zhong JH, Wang AL, Li GR, *et al.* $Co_3O_4/Ni(OH)_2$ composite mesoporous nanosheet networks as a promising electrode for supercapacitor applications. J Mater Chem, 2012, 22: 5656–5665
41 Gao Y, Mi L, Wei W, *et al.* Double metal ions synergistic effect in hierarchical multiple sulfide microflowers for enhanced supercapacitor performance. ACS Appl Mater Interfaces, 2015, 7: 4311–4319
42 Yu L, Zhang G, Yuan C, *et al.* Hierarchical $NiCo_2O_4@MnO_2$ core-shell heterostructured nanowire arrays on Ni foam as high-performance supercapacitor electrodes. Chem Commun, 2013, 49: 137–139
43 Yu D, Wu B, Ge L, *et al.* Decorating nanoporous ZIF-67-derived $NiCo_2O_4$ shells on a Co_3O_4 nanowire array core for battery-type electrodes with enhanced energy storage performance. J Mater Chem A, 2016, 4: 10878–10884
44 Zhang C, Geng X, Tang S, *et al.* $NiCo_2O_4$@rGO hybrid nanostructures on Ni foam as high-performance supercapacitor electrodes. J Mater Chem A, 2017, 5: 5912–5919
45 Xiao J, Yang S. Bio-inspired synthesis of NaCl-type $Co_xNi_{1-x}O$ ($0 \leq x < 1$) nanorods on reduced graphene oxide sheets and screening for asymmetric electrochemical capacitors. J Mater Chem, 2012, 22: 12253–12262
46 Qin T, Peng S, Hao J, *et al.* Flexible and wearable all-solid-state supercapacitors with ultrahigh energy density based on a carbon fiber fabric electrode. Adv Energ Mater, 2017, 6: 1700409
47 Zhao Y, Hu L, Zhao S, *et al.* Preparation of $MnCo_2O_4@Ni(OH)_2$ core-shell flowers for asymmetric supercapacitor materials with ultrahigh specific capacitance. Adv Funct Mater, 2016, 26: 4085–4093
48 Yuan C, Li J, Hou L, *et al.* Polymer-assisted synthesis of a 3D hierarchical porous network-like spinel $NiCo_2O_4$ framework towards high-performance electrochemical capacitors. J Mater Chem A, 2013, 1: 11145–11151
49 Wang R, Xia C, Wei N, *et al.* $NiCo_2O_4$@TiN core-shell electrodes through conformal atomic layer deposition for all-solid-state supercapacitors. Electrochim Acta, 2016, 196: 611–621
50 Wang Z, Zhu Z, Qiu J, *et al.* High performance flexible solid-state asymmetric supercapacitors from MnO_2/ZnO core-shell nanorods//specially reduced graphene oxide. J Mater Chem C, 2014, 2: 1331–1336
51 Zhai T, Lu X, Ling Y, *et al.* A new benchmark capacitance for supercapacitor anodes by mixed-valence sulfur-doped V_6O_{13-x}. Adv Mater, 2014, 26: 5869–5875
52 He Y, Chen W, Li X, *et al.* Freestanding three-dimensional graphene/MnO_2 composite networks as ultralight and flexible supercapacitor electrodes. ACS Nano, 2013, 7: 174–182
53 Liu J, Zhang L, Wu HB, *et al.* High-performance flexible asymmetric supercapacitors based on a new graphene foam/carbon nanotube hybrid film. Energ Environ Sci, 2014, 7: 3709–3719

Acknowledgements This work was supported by the National Natural Science Foundation of China (61376011), Gansu Provincial Natural Science Foundation of China (17JR5RA198) and the Fundamental Research Funds for the Central Universities (lzujbky-2017-k21).

Author contributions Hao J and Qin T designed and fabricated the materials and devices, analyzed the results, and wrote the manuscript. Wang Z and Wen Y drew the schematic illustration and figures. Peng S and Cao G supervised the project and revised the manuscript. All authors contributed to the general discussion.

Conflict of interest The authors declare that they have no conflict of interest.

Supplementary information Supporting data are available in the online version of the paper.

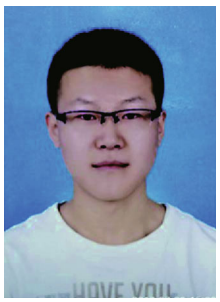

Jiaxin Hao is a graduate student at Lanzhou University. His current research is focused on the design and optimization of electrode materials for energy storage.

Shanglong Peng received his BSc degree (2003) in Physics and PhD degree (2008) in Condensed Matter Physics from Lanzhou University. He is currently a professor at School of Physical Science and Technology, Lanzhou University. His current research is focused on the design of advanced electronic and energy materials, and control of surface and interface properties in energy related applications, mainly including solar cells and supercapacitor.

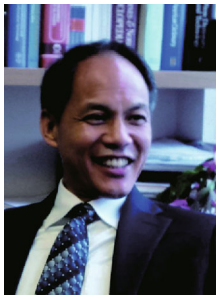

Guozhong Cao is a boeing-steiner professor of Materials Science and Engineering, Professor of Chemical Engineering, and Adjunct Professor of Mechanical Engineering at the University of Washington, Seattle, US. His current research is focused on chemical processing of nanomaterials for energy related applications including solar cells, rechargeable batteries, supercapacitors and hydrogen storage.

电化学离子交换法辅助制备可用作高性能超级电容器电极的$Co_3O_4/NiCo_2O_4$纳米复合材料

郝加新[1], 彭尚龙[1*], 秦天锋[1], 王子磊[1], 温昱祥[1], 贺德衍[1], 张加驰[1], 张稚雅[1], 范晓彦[2], 曹国忠[3*]

摘要 离子交换技术被广泛用于调节过渡金属氧化物的成分, 采用该技术制备的超级电容器电极材料, 在保持其形貌的同时能增加其比容量. 本文报道了一种新颖的电化学方法辅助制备复合$Co_3O_4/NiCo_2O_4$纳米材料. 通过电化学离子交换, 可以将Ni^{2+}快速引入并部分替换Co_3O_4纳米材料中的Co^{2+}, 从而得到Co_3O_4和$NiCo_2O_4$的复合纳米材料. 将其用作超级电容器正极材料, 在5 mA cm^{-2}的电流密度下, 其面电容达到了3.2 F cm^{-2}, 并展现出了良好的倍率性能及优异的循环稳定性. 此外, 两个串联的非对称器件($Co_3O_4/NiCo_2O_4$//碳布)在充电3 min后可以将10个并联的绿色LED点亮大约6 min, 展现出良好的实用性.